Preprints of the 21st IFAC World Congress (Virtual)
Berlin, Germany, July 12-17, 2020

Systematic calibration of a simulated semi-autogenous/ball-mill grinding circuit

E.M. Pérez-García * **J. Bouchard** *,** **É. Poulin** *,***

* *Université Laval, LOOP, Centre E4m, Pavillon Adrien-Pouliot, 1065 avenue de la médecine, Québec, Québec, Canada, G1V 0A6*
Corresponding author: edgar.perez.1@ulaval.ca
** *Département de génie chimique*
*** *Département de génie électrique et de génie informatique*

Abstract: With no doubt, modeling and simulation are powerful tools improving the performance of current optimisation and control strategies. At least in the mineral processing field, however, one of the major gaps in literature is that authors frequently skip specific details on the model calibration methodologies, mainly those concerning data acquisition and processing, calibration sequence, cost function formulation (including constraints), optimisation problem solution, parameter uncertainty, etc. As a contribution to that matter, this paper presents a detailed calibration procedure for a grinding circuit model from plant and laboratory data. The methodology integrates both a global search routine to avoid cost function local minima, and a Jack-knife resampling and recalibration technique to estimate the parameter confidence. The simulator will serve in future work for the coupling of separation processes, and thus the development of plant-wide model-based optimisation and control strategies.

Keywords: Identification and modelling; process observation and parameter estimation; advanced process control.

1. INTRODUCTION

Computer simulation of grinding circuits has multiple industrial purposes, e.g. equipment design, personnel training, and obviously optimisation and control. According to a review conducted by Rogers et al. (2019), automation is improving the value chain of the mineral industry (from exploration to refining) as never before. Most strategies rely currently on simple PID controllers that achieve acceptable performances. However, model-based approaches have already demonstrated considerable advantages in terms of throughput, fluctuations in the key variables, recovery, and product quality, to name a few (Bouffard, 2015).

Although model calibration is key for the success of the mentioned purposes, this stage still faces several obstacles hindering the development of standardised methodologies. The main gap in the literature is not the lack of data or dynamic models, but rather to a shortfall of specific information detailing data acquisition and processing, calibration sequence, cost function formulation and constraints, optimisation problem solution, parameter uncertainty, etc.

Using both plant and laboratory data, Légaré et al. (2016a) developed an approach that initialises the dynamic calibration with a steady-state solution. Inspired by their work, this paper details the step-by-step calibration of a grinding circuit model with a special emphasis on aforementioned specific technical information. Section 2 presents the actual circuit and the derived mathematical models. The methodology proposed in Section 3 integrates a global search optimisation routine to avoid cost function local minima. Additionally, a Jack-knife resampling strategy was adapted to provide an estimate of the parameter uncertainty. The results and discussion in Section 4 give the model parameters as well as the comparison between simulated and measured data.

2. CIRCUIT AND MODEL

IAMGOLD Corporation operates Westwood mine located in northwestern Quebec, Canada. The grinding circuit, represented in Figure 1, comprises a semi-autogenous (SAG) mill and a ball mill (BM). Both mills operate in closed circuit with separate hydrocyclone clusters. Water is added independently to each mill as well as to each pump box for level control. The final product undergoes a gold leaching process. The following subsections introduce the different models used to build the plant simulator.

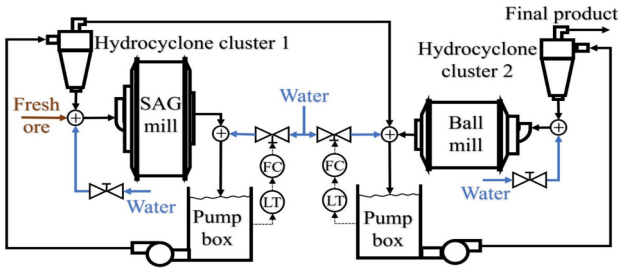

Fig. 1. Westwood grinding circuit.

2.1 Semi-autogenous mill model

The grinding process in a SAG mill as described by Sbárbaro (2010) is

$$\frac{\mathrm{d}\mathbf{w}_h}{\mathrm{d}t} = \dot{\mathbf{w}}_f - \dot{\mathbf{w}}_p + \frac{W_P}{w_h}\left(-\mathbf{S}\mathbf{w}_h + \mathbf{B}\mathbf{S}\mathbf{w}_h\right) \tag{1}$$

where $\mathbf{w}_h$ is the hold-up vector sorted by size classes, $\dot{\mathbf{w}}_f$ and $\dot{\mathbf{w}}_p$ are the feed and product flow rate vectors respectively, w_h is the total ore hold-up and W_P is the mill power draw. $\mathbf{S}$ is the selection function, a diagonal matrix providing the fragmentation rates for every particle size. The breakage matrix $\mathbf{B}$ is a lower triangular matrix where each column is the fractional distribution of the generated fragments into size classes. The ore discharge rate is

$$\dot{\mathbf{w}}_p = k_p \mathbf{C} \frac{\mathbf{w}_h}{\sqrt{w_h}} \tag{2}$$

where k_p is a calibration constant, and $\mathbf{C}$ is a classification diagonal matrix dependent of the mill grate design and the charge solids fraction Φ. The water discharge rate

$$\dot{Q}_f = \left(k_{w0} + \frac{k_{w1}}{w_h^4}\right) w_w \tag{3}$$

features two calibration parameters k_{w0} and k_{w1}, and depends on both the ore hold-up and water hold-up w_w.

Due to a square aspect ratio, i.e. $L \approx D$, and ball charge of 19% V/V, the mill exhibits a hybrid behaviour combining both SAG and ball mills characteristics. The power draw

$$W_P = W_E + k_M W_M + k_{A1} D^{2.5} L\,(1 - k_{A2}\nu)\, f(N_c)\rho_h \tag{4}$$

is thus better captured when combing two models, as each one associates to a specific feature. W_E is the no-load power (i.e. the theoretical consumption when the mill is empty) and W_M obeys to a highly detailed description of the charge movement and shape inside the mill (Morrell, 1993). The remaining terms come from a SAG mill specific model (Austin, 1990) depending on the mill length L and diameter D, filling fraction ν, a function of the mill critical speed (i.e. the speed at which no grinding occurs) ratio N_c and density of the charge ρ_h. Only the empirical parameters k_M, k_{A1} and k_{A2} require calibration.

The diagonal of $\mathbf{S}$ comes from interpolating the size classes vector $\mathbf{d}_p$ within the cubic spline fitting $(d_{p,1}, s_0)$, $(d_{p,min}, s_{min})$, $(d_{p,max}, s_{max})$ and $(d_{p,n}, s_n)$ where $d_{p,1} > d_{p,min} > d_{p,max} > d_{p,n}$. The curve displays a rotated-s trend characteristic of this type of mill, so the subindexes max and min refer to the interior maximum and minimum of the spline, respectively. The coefficients s_0, s_{min}, s_{max}, s_n, $d_{p,min}$ and $d_{p,max}$ need calibration while $d_{p,1}$ and $d_{p,n}$ are simply the first and last elements in $\mathbf{d}_p$. Pérez-García et al. (2019) detail the relationship between the curve shape, calibration parameters and physical process. As for the $\mathbf{B}$ matrix, the cumulative fraction of mass going to size class i when a particle of size j breaks is

$$b_{i,j} = \begin{cases} \varphi_i \left(\dfrac{d_{p,i}}{d_{p,j}}\right)^{\beta_B} + (1-\varphi_i)\left(\dfrac{d_{p,i}}{d_{p,j}}\right)^{\gamma_B} & \text{if } i > j \\ 0 & \text{if } i \leq j \end{cases} \tag{5}$$

with

$$\varphi_i = \varphi_0 \left(\frac{d_{p,i}}{d_{p,1}}\right)^{\delta_B} \tag{6}$$

and ore-specific calibration parameters β_B, γ_B, δ_B and φ_0, assumed independent of the grinding environment.

2.2 Ball mill model

The ball mill model, as described by Légaré et al. (2016b), supposes grinding to be independent of W_P and w_h, i.e.

$$\frac{\mathrm{d}\mathbf{w}_h}{\mathrm{d}t} = \dot{\mathbf{w}}_f - \dot{\mathbf{w}}_p - \mathbf{S}\mathbf{w}_h + \mathbf{B}\mathbf{S}\mathbf{w}_h \tag{7}$$

with the same breakage function in (5). The $\mathbf{S}$ matrix differs though, and the elements on the diagonal are

$$s_{i,i} = \frac{S_0 d_{p,i}^{\alpha_s}}{1 + (d_{p,i}/x_m)^{\sigma_s}} \tag{8}$$

with

$$x_m = 0.2971 \exp(0.0346 D_b) \tag{9}$$

where S_0, α_s and σ_s are calibration parameters, and D_b is the grinding media top size.

The material flows through as a series of continuously stirred tank reactors with independent behaviour, breakage, and internal classification functions. The slurry transport depends of two volume parameters V_d and V_f, and a rheology factor Ω requiring calibration. The power model is (4) with $k_{A1} = 0$, i.e. only the ball mill component.

2.3 Hydroclyclones

Along with geometry and number of active units, the hydrocyclone model (Plitt, 1976) includes four calibration parameters C_{h1}, C_{h2}, C_{h3}, and C_{h4}, influencing the

- d_{50}, i.e. the size of a particle having the same probability of going to the underflow or the overflow;
- pressure drop P that depends on the inlet flow rate;
- volumetric flow rate distribution between the underflow and overflow; and
- classification efficiency, respectively.

2.4 Auxiliary equipment

A conveyor belt delivers the fresh ore following a first order dynamics for speed variations. The time constant is adjusted prior to circuit calibration to match the measured feed rate. The ore properties are delayed based on length and speed to account for the material that remains on the belt after any alteration in the feed. Pipes connecting the pump boxes with the hydrocyclones also delay the ore properties based on the internal volume and the pulp volumetric flow rate, which is always the same in the inlet and outlet (assumed incompressible). The pump boxes are modeled as perfectly mixed tanks, and water addition controls the level. Constant pump speed and perfect level control (i.e. water addition reacts to pulp flow variations instantaneously so the level remains constant) are assumed for model calibration.

3. CALIBRATION PROCEDURE

3.1 Plant sampling and laboratory test work

For the mill discharges, and the hydrocyclone underflow and overflow streams, an initial pulp sample was cut assuming steady state at nominal operating conditions. The solids fraction was measured with on-site Marcy scales. The ore feed rate to the SAG mill was increased from 108 t/h to 123 t/h, and the streams resampled every fifteen minutes approximately. Afterwards, the water feed rate was changed from 38 m^3/h to 45 m^3/h and the sampling repeated. Personnel availability and circuit configuration limited the sampling rate. The 15-min period may seem long to assess the transient responses, but the purpose here is essentially to calibrate the size of the mill model reactors and the $\mathbf{S}$ matrices. Online data from to the testing period was extracted from the historical log, including the SAG mill feed rates, power draw, bearings pressure, water addition to the first pump box, and the pressure drop in both hydrocyclone clusters. An empirical relationship based on the personnel experience is established between the SAG mill bearings pressure and filling level. This power draw and mill filling are not available online for the ball mill, so they are only compared to nominal values. Collecting validation data and samples was not possible.

All the pulp samples were filtered and dried. Particle size distribution (PSD) was measured by dry sieving except for the -38 μm fraction, which was screened in wet. Sampling the SAG mill feed was not possible, so size distribution was determined from historical measurements. Additionally, five dry samples from the crusher product were prepared for single-size batch grinding tests (Austin et al., 1984), namely $-6.73/+4.76$ mm, $-2.38/+1.68$ mm, $-1.68/+1.19$ mm, $-850/+600$ µm, and $-300/+212$ µm. Every sample was dry ground in three cycles of five minutes each inside a 9000 cm^3 square mill filled with 3.8 cm diameter steel balls at 19% V/V. PSD was measured after each cycle. For the last two samples, only the remaining particles of top size were weighted for practicality, as they are considerably fine already with a narrow distribution.

3.2 Breakage function calibration

The consumption rate was calculated for the top size of the five samples fitting the remaining mass to a first order kinetic expression. A matrix $\mathbf{S}$ as in (8) was then calibrated with the parameters S_0, α_s, and σ_s. Using (7) with $\dot{\mathbf{w}}_f = \dot{\mathbf{w}}_p = 0$, the ore breakage parameters $\{\beta_B, \gamma_B, \delta_B, \varphi_0\} \in \boldsymbol{\theta}_B$ in (5) were calibrated to fit the measured size distribution curves. The parameters were estimated through unconstrained iterative nonlinear least squares, and the uncertainties $\boldsymbol{\sigma}_{\theta_B}$ extracted from the covariance matrix of the cost function

$$J_B = \sum_{t=1}^{3} \sum_{s=1}^{n_s} \frac{1}{n_i} \sum_{i=1}^{n_i} \left(F_{i,s,5t} - \hat{F}_{i,s,5t} \right)^2 \qquad (10)$$

where the measured and predicted cumulative size distributions $F_{i,s,5t}$ and $\hat{F}_{i,s,5t}$ are compared for every five minute grinding cycle of the sample s. For dynamic calibration, $\boldsymbol{\theta}_B$ remains fixed as it is ore-dependent. Contrarily, the laboratory-determined $\mathbf{S}$ is only valid for the batch mill, so it must be discarded then recalibrated.

3.3 Dynamic model calibration

The cost function for the SAG and ball mill sections is

$$J = \frac{1}{n_k} \sum_{k=1}^{n_k} \left[\left(W^*_{P,k} - \hat{W}^*_{P,k} \right)^2 + \left(\nu^*_k - \hat{\nu}^*_k \right)^2 + \left(P^*_k - \hat{P}^*_k \right)^2 \right] + \sum_{f=1}^{n_f} \left\{ \frac{1}{n_s} \sum_{s=1}^{n_s} \left[\left(\Phi^*_{s,f} - \hat{\Phi}^*_{s,f} \right)^2 + \frac{1}{n_i} \sum_{i=1}^{n_i} \left(F^*_{i,s,f} - \hat{F}^*_{i,s,f} \right)^2 \right] \right\} \qquad (11)$$

where n_k, n_f, and n_s are the number of online observations, streams, and samples per stream, respectively. The superscript * denotes normalisation between 0 and 1 accordingly to the highest and lowest measured values. In this way, model calibration relies in an iterative nonlinear least squares minimisation routine to solve

$$\theta = \arg\min J \text{ s.t. } \begin{cases} \mathbf{A}_J \theta \leq \mathbf{b}_J \\ \theta_{\min} \leq \theta \leq \theta_{\max} \end{cases} \qquad (12)$$

where $\mathbf{A}_J$ and $\mathbf{b}_J$ define constraints concerning the SAG mill $\mathbf{S}$ matrix while $\theta_{\min}$ and $\theta_{\max}$ are the parameter lower and upper bounds, respectively. These were chosen empirically so the behaviour of the model remained realistic.

The procedure was divided in three stages. Firstly, the circuit was separated in the SAG mill and ball mill sections and they were independently calibrated in steady-state to produce an initial estimate of the calibration parameters $\boldsymbol{\theta}_0$. Secondly, the complete circuit was calibrated considering dynamics and initialised with $\boldsymbol{\theta}_0$, resulting the solution $\boldsymbol{\theta}$ (see Section 4.2). Lastly, the parameter uncertainty was estimated. Due to the problem constraints, the covariance matrix could not be suitable to estimate parameter uncertainties in some situations, e.g. when the solution is near the imposed bounds. Jack-knife resampling offers an alternative to get an estimate of the parameter uncertainty in dynamic models (Duchesne and MacGregor, 2001). The optimisation problem is solved n_s additional times using "jack-knifed" data sets, i.e. simulating the effect of missing one sample each time. The online data in the vicinity of the corresponding sampling instant is also omitted. This technique generates biased replicates of the calibration parameters and thereby the possibility to calculate a standard deviation $\boldsymbol{\sigma}_\theta$. Figure 2 summarises the proposed procedure, including the laboratory test work. Section 4 discusses the outcomes of this approach, comprising the calibrated parameters and uncertainties, as well as the comparison between measured and simulated variables.

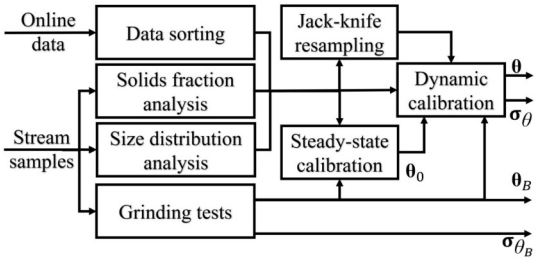

Fig. 2. Model calibration procedure.

4. RESULTS AND DISCUSSION

Laboratory results are first introduced. Then follows the parameter calibration results, and a discussion about parameter uncertainties, and the comparison between measured and simulated variables.

4.1 Breakage function calibration

Table 1 gathers the parameters determined after the grinding tests. As discussed before, the selection function parameters depend on the mill, while the breakage function ones are ore-characteristic dependent. Although all of them are statistically significant according to the standard deviations, the mill parameters are less precise. This can be explained after analysing the measurements and predictions, but it must be emphasised again that the simulation model only uses the ore parameters.

Table 1. Laboratory-determined grinding parameters.

Mill			Ore		
Par.	Value	S.D. [%]	Par.	Value	S.D. [%]
S_0	0.1477	8.12	β_B	0.1991	4.42
α_S	1.1370	34.18	γ_B	5.9019	9.53
σ_S	1.1490	29.58	δ_B	0.3429	6.79
			φ_B	0.4258	3.33

Note: S.D. is given in percentage of the estimated value.

For the five samples ground in laboratory, Figure 3.a follows the mass consumption of the top size particles. These curves allowed in turn to determine consumption rates, which correspond to the measured points in Figure 3.b. As expected, the finer particles are likely to consume at lower rates due to several phenomena, such as the probability of impact inside the mill, and fewer available microfractures. This graph also shows that the calibrated selection function represents the fragmentation kinetics adequately. The relatively high uncertainties in Table 1 may be a consequence of the lack of measurements for the very fine sizes, allowing this portion of the curve to vary (as the parameters do so) without any significant effect on the right-hand side of the curve. Figure 3.c illustrates how the size distribution evolves as the grinding cycles progress. For practicality, only the three samples with larger particles, and thus a more dispersed distribution, were sieved. As the top size decreases, the size distribution varies less with each cycle. This is a consequence of the slower consumption rates of smaller particles. The grinding model captures progression satisfactorily over the entire range of particle sizes.

4.2 Dynamic model calibration

Table 2 lists the calibration parameters θ in two columns, the left one corresponds to the SAG mill section, and the right one to the ball mill section. Global search ensures that this is not a local minimum solution, as it initialises the problem multiple times with different parameter combinations. Moreover, all the parameters are statistically significant according to their uncertainty, adding to the confidence in the validity of the solution. Note again that deviations are estimated by Jack-knife resampling and recalibration. In general, the SAG mill section parameters have smaller uncertainties, probably because the grinding dynamics is dependent of power consumption and charge, having thus less freedom to vary as several variables are touched simultaneously.

Figure 4.a shows the mill ore and water feed changes applied. The ore feed rate does not follow a step, it increases and decreases before it settles to the final value, only after more water is added to the mill. The mill charge initially follows the feed rate fluctuations, as seen in Figure 4.b, it recovers following the feed water increase, which promotes mass transport.

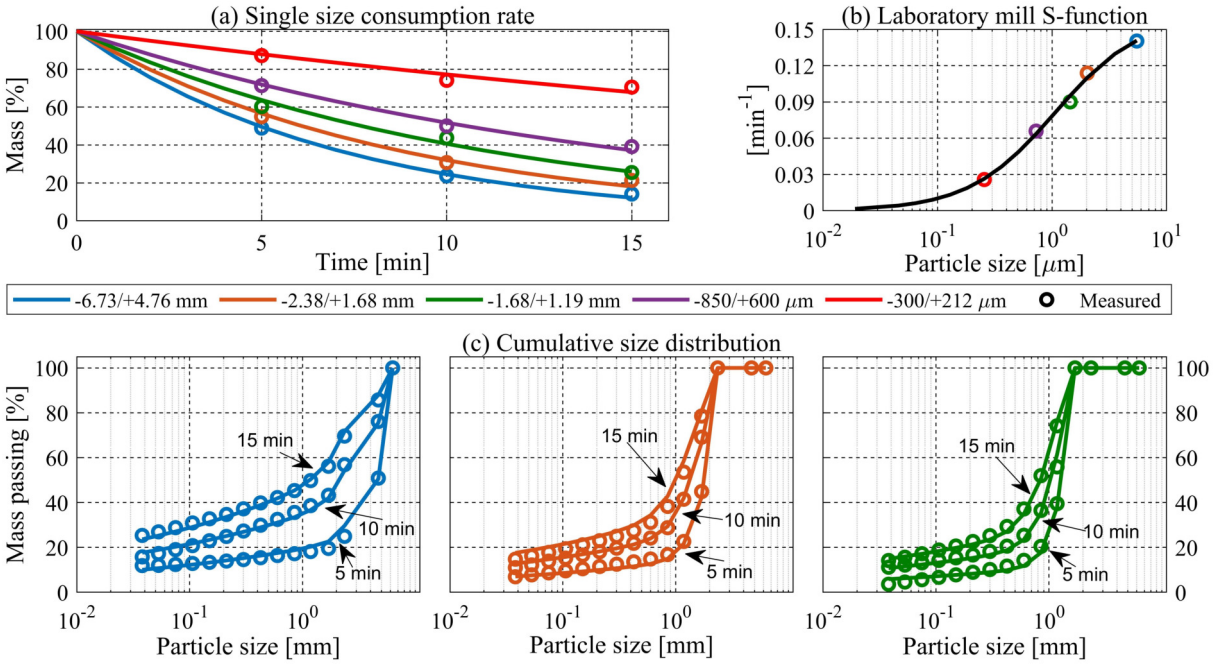

Fig. 3. Laboratory test work results.

Table 2. Model calibration parameters θ.

SAG flow			BM flow		
Par.	Value	S.D. [%]	Par.	Value	S.D. [%]
k_p	37.1571	1.0375	V_d	15.9650	16.4494
k_{w0}	9.2604	1.9301	V_f	10.0320	12.8323
k_{w1}	0.2883 $\times 10^6$	7.1177	Ω	8.3689	19.3695
SAG grinding			**BM grinding**		
Par.	Value	S.D. [%]	Par.	Value	S.D. [%]
s_0	0.0536	6.4174	S_0	0.7923	14.0377
s_{max}	0.8452	1.3885			
s_{min}	0.6985	1.3308	α_s	0.6260	12.9674
s_n	6.9720	0.7958			
d_{max}	3.2225	3.4358	σ_s	2.8653	9.7820
d_{min}	27.6926	0.6312			
SAG power			**BM power**		
Par.	Value	S.D. [%]	Par.	Value	S.D. [%]
k_M	0.5093	0.2774			
k_{A1}	38.8987	0.1524	k_M	0.7728	1.2277
k_{A2}	3.8784	0.1526			
Hydrocyclone cluster 1			**Hydrocyclone cluster 2**		
Par.	Value	S.D. [%]	Par.	Value	S.D. [%]
C_{h1}	0.4733	13.0228	C_{h1}	1.6067	14.6164
C_{h2}	0.0322	2.9456	C_{h2}	0.0196	9.2036
C_{h3}	0.2553	5.2004	C_{h3}	0.2299	1.7863
C_{h4}	0.4214	3.1861	C_{h4}	0.5698	5.5437

Note: S.D. is given in percentage of the estimated value.

Figure 4.c depicts an acceptable fit between measured and simulated power consumption, capturing the negative correlation with the feed rate. It drops as the mass in the mill builds up and vice versa. In the actual operation, this may occur when the hold-up level is such that the mill cannot lift the slurry efficiently, affecting the centre of mass and consequently the rotational inertia.

Figure 4.d displays the PSD of the different streams for this section of the circuit. Each curve of the same stream corresponds to a different sampling time. The P_{80} (i.e. the sieve size through which 80% of the mass can pass), P_{60} and P_{50} indexes are reproduced in Figure 4.e. Except for the underflow P_{80}, the calibrated model reproduces size distributions. Lastly, the solids fraction of the underflow stream also present some discrepancies, as seen in Figure 4.f. Sampling some streams, including this one, was challenging due to the physical configuration, thus increasing the sampling error. As mentioned before, the size distribution of the SAG mill feed was determined from historical measurements, and remained constant for calibration. Knowing the actual size distribution and its variations during tests would certainly improve the fit.

For the ball mill section, Figures 5.a, 5.b, and 5.c report the size distributions, P_{80} and P_{50} indexes, and solids fraction, respectively. The ball mill section displays less measured data, i.e. power draw and filling missing, and tighter size distributions as the material is finer. The general trends are well captured but there are some discrepancies between the measured and simulated values. As the circuit is dynamically calibrated as a whole, the errors in the SAG mill section propagate through the stream connecting the system. Furthermore, measurement errors are more likely to occur with smaller particle sizes, especially for dry manipulations as it is the case here.

In the light of these results, the simulated grinding circuit appears to be able to reproduce the behaviour of the actual one. Note that for process control applications, the overall trends are more important than the precise prediction of given variables. The presented calibration methodology therefore seems to be adequate to develop a comprehensive model for such developments. Unfortunately, collecting a second data set to reinforce this conclusion was impossible due to logistic and manpower issues.

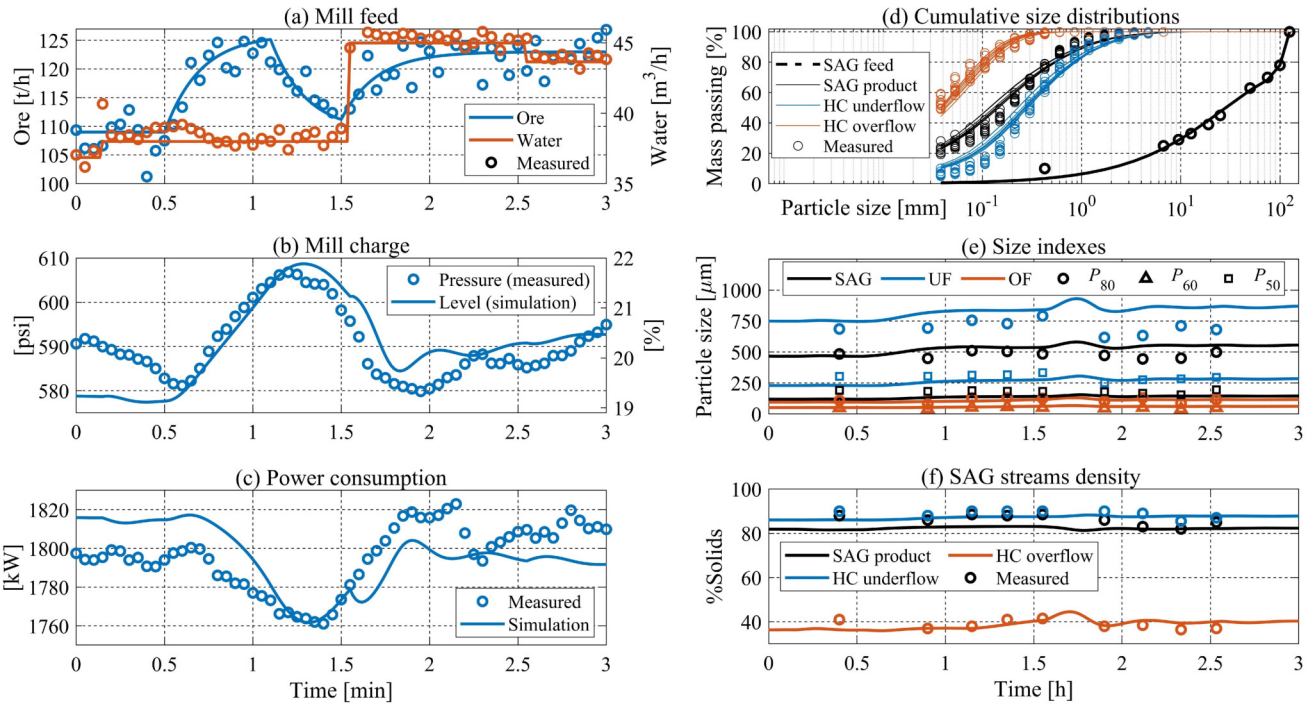

Fig. 4. Fit of the model SAG section after calibration.

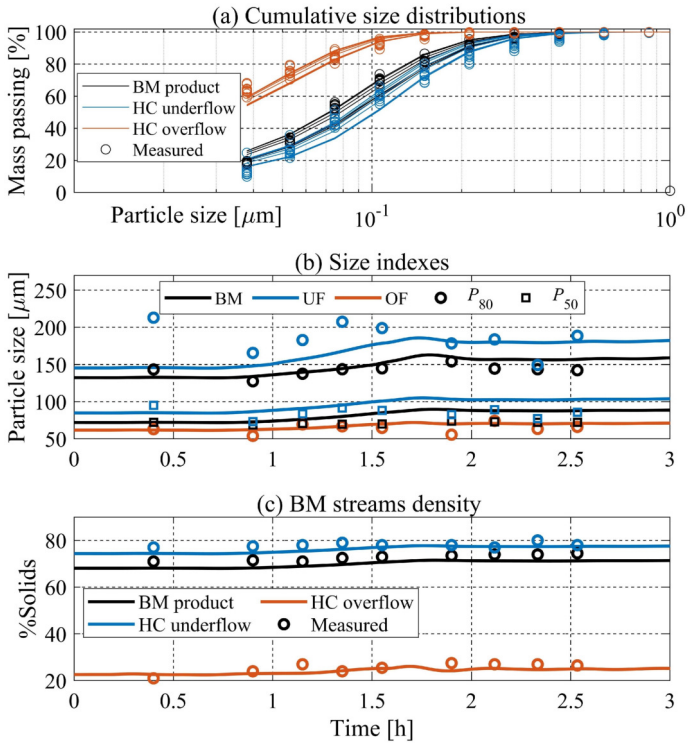

Fig. 5. Fit of the model ball mill section after calibration.

5. CONCLUSION

This paper presented a calibration procedure for a grinding circuit model, integrating global search and Jack-knife recalibration approaches to ensure the solution confidence. The results and discussion lead to the following conclusions: 1) the grinding circuit simulator can reproduce the behaviour of the actual plant with acceptable precision, allowing its future use in developing model-based optimisation and control strategies; 2) the Jack-knife resampling and recalibration approach provides estimates of the parameter precision; 3) the calibration parameter uncertainties, along with the use of a global search approach, add to the confidence in the validity of the solution, and; 4) providing the details of the whole calibration procedure contributes to fill the gap in the literature.

The quality of the fit, and thus the reproducibility of the model, can only improve as more measurements with higher precision are available, including online data and laboratory test work. Implementing dedicated sampling accesses and equipment and installing properly calibrated sensors for all key variables in the actual plant, would ensure the collection of more reliable data. Moreover, this would contribute to the task of efficiently updating the model parameters periodically, thus preserving its validity over time. Regarding laboratory work, wet grinding and sieving could also enhance the precision when assessing size distributions, however, substantially more time is required as a result of the drying periods. The number and size of the samples, as well as the available laboratory equipment, are aspects to be equally taken into account.

As the main goal of grinding is the separation of valuable minerals, future work will address the coupling of separation processes to the grinding circuit model for the development and testing of plant-wide optimisation and control strategies in simulation. The authors recall that the primary focus of this paper is the thoroughness of the calibration procedure itself rather than that of data collection, but if the commissioning of such strategies in the actual plant was considered, measuring the circuit feed PSD would be unavoidable to ensure representativeness.

ACKNOWLEDGEMENTS

The authors acknowledge CONACYT-Mexico (PhD scholarship number 440297), as well as FRQNT and Fonds vert in Quebec for the financial support. Thanks also to Hafedh Tbaybi, Jr Metallurgist at IAMGOLD Corporation, for the support during the sampling campaign. Special thanks are due to Alex Thivierge, Mohammad Asif, and Vicky Dodier for plant and laboratory work.

REFERENCES

Austin, L.G. (1990). A mill power equation for SAG mills. *Minerals and Metallurgical Processing*, 7(1), 57–63. doi: https://doi.org/10.1007/BF03403284.

Austin, L., Klimpel, R., and Luckie, P. (1984). *Process Engineering of Size Reduction: Ball Milling*. SME, New York, U.S.A.

Bouffard, S.C. (2015). Benefits of process control systems in mineral processing grinding circuits. *Minerals Engineering*, 79, 139–142. doi: https://doi.org/10.1016/j.mineng.2015.06.006.

Duchesne, C. and MacGregor, J.F. (2001). Jackknife and bootstrap methods in the identification of dynamic models. *Journal of Process Control*, 11(5), 553–564. doi: https://doi.org/10.1016/S0959-1524(00)00025-1.

Légaré, B., Bouchard, J., Clapperton, A., Poulin, É., and Rojas-Montes, J.C. (2016a). Calibration of a dynamic model for industrial comminution circuit. In *Proceedings of the XXVIII International mineral processing congress*. Quebec City, Canada.

Légaré, B., Bouchard, J., and Poulin, É. (2016b). A modular dynamic simulation model for comminution circuits. *IFAC-PapersOnLine*, 49(20), 19–24. doi: http://dx.doi.org/10.1016/j.ifacol.2016.10.090.

Morrell, S. (1993). *The Prediction of Power Draw in Wet Tumbling Mills*. PhD thesis, University of Queensland, Queensland, Australia.

Pérez-García, E.M., Bouchard, J., and Poulin, É. (2019). Development and calibration of an autogenous/semi-autogenous mill simulation model for process control applications. In *Proceedings of the LVIII annual Conference of Metallurgists*. Vancouver, Canada.

Plitt, L. (1976). A mathematical model of the hydrocyclone classifier. *CIM Bulletin*, 69(776), 114–123.

Rogers, W.P., Kahraman, M.M., Drews, F.A., Powell, K., Haight, J.M., Wang, Y., Baxla, K., and Sobalkar, M. (2019). Automation in the mining industry: Review of technology, systems, human factors, and political risk. *Mining, Metallurgy & Exploration*, 36(607). doi: http://10.1007/s42461-019-0094-2.

Sbárbaro, D. (2010). Dynamic simulation and model-based control system design for comminution circuits. In *Advanced Control and Supervision of Mineral Processing Plants*, chapter 5, 213–245. Springer, London, England.